INTERNATIONAL JOURNAL OF HEAT AND TECHNOLOGY
Vol.33 (2015), No.3, pp.79-84
http://dx.doi.org/10.18280/ijht.330311

THE EFFECT OF GEOMETRICAL PARAMETERS ON ENHANCING THE HEAT TRANSFER INSIDE A MICROTUBE

B. H. Salman*,[1], H. A. Mohammed[2], A. SH. Kherbee[3] and Hamdi E. Ahmed[4]

[1] Department of Mechanical Engineering, University of Nevada, Las Vegas, 89154 NV, USA;
[2] Department of Thermofluids, Universiti Teknologi Malaysia, 81310 UTM Skudai, Johor Bahru, Malaysia;
[3] Mechanical Engineering Department, Universiti Tenaga Nasional, 43000 Kajang, Selangor, Malaysia;
[4] Department of Mechanical Engineering, University of Anbar, 31001 Anbar, Iraq.

Email: eng.bassam2007@yahoo.com

ABSTRACT

In this paper, the effect of geometrical parameters of microtube on enhancing the heat transfer has been studied numerically. Single phase model was used to simulate the flow of sio_2-ethlyen glycol nanofluids inside a microtube at different reynolds numbers ranged from 10 to 160 at constant heat flux boundary condition. The results show that the higher tube diameter and entrance size has the highest Nusselt number and lower pressure drop. Furthermore, no effect of inclination angles was found.

Keywords: Numerical modelling, Nanofluids, Microtube, Heat transfer enhancement.

1. INTRODUCTION

In recent years, liquid suspensions containing nanoparticles gained significant attention in science and engineering. Their unique thermophysical properties, such as a drastically reduced melting temperature of the nanoparticles compared to their bulk counterpart [1, 2], allow for novel methods in the manufacturing of nano and microelectronic devices. Many researchers intended to investigate experimentally and numerically the effects of the microtube and microchannel shapes, sizes, heat transfer and the other parameters that can be influence on the performance for the microelectronic devices. However, the recent numerical and experimental researches that related to microtube have been summarized in Table1.

The purpose of this work is to provide a numerical study on the effect of geometrical parameters (entrance size, shape and inclination angle on enhancing the heat transfer at different Reynolds number ranged from 10 to 120 for different inclination angles ranged from 0 °to ±90 °.

2. NUMERICAL MODEL

2.1 Geometry and the governing equations

Navier–Stokes and energy equations were used to describe the flow and heat transfer in the microtube. The following assumptions are adopted: (i) The nanofluid is incompressible, the flow is laminar, the radiation heat transfer effects are negligible; (ii) The nanoparticles are assumed to be spherical and single phase model is used; (iii) Constant thermophysical properties are considered for the nanofluid. The governing equations used are as follows:

Continuity equation:

$$\frac{1}{R}\frac{\partial}{\partial\theta}(\rho_{eff}U)+\frac{1}{R}\frac{\partial}{\partial R}(\rho_{eff}RV)+\frac{\partial}{\partial Z}(\rho_{eff}W)=0 \quad (1)$$

Momentum equation:
θ-components

$$\frac{1}{R}\frac{\partial}{\partial\theta}(\rho_{eff}UU)+\frac{1}{R}\frac{\partial}{\partial R}(\rho_{eff}RVU)+\frac{\partial}{\partial Z}(\rho_{eff}WU)+\frac{1}{R}(\rho_{eff}UV)$$
$$=-\frac{1}{R^2}\frac{\partial P}{\partial\theta}+\frac{1}{R^2}\frac{\partial}{\partial\theta}\left(\mu_{eff}\frac{\partial U}{\partial\theta}\right)+\frac{\partial}{\partial R}\left(\frac{\mu_{eff}}{R}\frac{\partial(RU)}{\partial R}\right)+\frac{2\mu_{eff}}{R^2}\frac{\partial V}{\partial\theta} \quad (2a)$$

R- Components

$$\frac{1}{R}\frac{\partial}{\partial\theta}(\rho_{eff}UV)+\frac{1}{R}\frac{\partial}{\partial R}(\rho_{eff}RVV)+\frac{\partial}{\partial Z}(\rho_{eff}WV)-\frac{1}{R}(\rho_{eff}U^2)$$
$$=-\frac{1}{R}\frac{\partial P}{\partial\theta}+\frac{1}{R^2}\frac{\partial}{\partial\theta}\left(\mu_{eff}\frac{\partial V}{\partial\theta}\right)+\frac{\partial}{\partial R}\left(\frac{\mu_{eff}}{R}\frac{\partial(RV)}{\partial R}\right)-\frac{2\mu_{eff}}{R^2}\frac{\partial U}{\partial\theta} \quad (2b)$$

Z- Components

$$\frac{1}{R}\frac{\partial}{\partial\theta}(\rho_{eff}UW)+\frac{1}{R}\frac{\partial}{\partial R}(\rho_{eff}RVW)+\frac{\partial}{\partial Z}(\rho_{eff}WW)$$
$$=-\frac{\partial P}{\partial Z}+\frac{1}{R^2}\frac{\partial}{\partial\theta}\left(\mu_{eff}\frac{\partial W}{\partial\theta}\right)+\frac{1}{R}\frac{\partial}{\partial R}\left(R\mu_{eff}\frac{\partial W}{\partial\theta}\right) \quad (2c)$$

Energy equation:

$$\frac{1}{R}\frac{\partial}{\partial\theta}(\rho_{eff}U\Theta)+\frac{1}{R}\frac{\partial}{\partial R}(\rho_{eff}RV\Theta)+\frac{\partial}{\partial Z}(\rho_{eff}W\Theta)$$
$$=\frac{1}{R^2}\frac{\partial}{\partial\theta}\left(\frac{K_{eff}}{(C_p)_{eff}}\frac{\partial\Theta}{\partial\theta}\right)+\frac{\partial}{R\partial R}\left(R\frac{K_{eff}}{(C_p)_{eff}}\frac{\partial\Theta}{\partial R}\right) \quad (3)$$

Where the non-dimensional variables are defined as

$$R = \frac{r}{D},\ Z = \frac{z}{D},\ U = \frac{u}{u_\infty},\ V = \frac{v}{u_\infty},\ W = \frac{w}{u_\infty},\ \Theta = \frac{T-T_\infty}{T_w-T_\infty},\ P = \frac{p}{\rho u_\infty^2}$$

The ρ_{eff} , μ_{eff} , C_{eff} and k_{eff} are density, viscosity, heat capacity and thermal conductivity of nanfluid, respectively.

2.2 Boundary conditions

At the tube inlet, the inlet temperature was taken as T_{in}=301 K. No-slip conditions and uniform heat flux used was 50000 W/m^2 to heat up the tube. Different velocities depending on the values of Reynolds number were used. At the tube outlet, the flow and heat transfer are assumed to be fully developed.

2.3 Nanofluids thermophysical properties

The thermophysical properties which are density, heat capacity, dynamic viscosity and thermal conductivity for SiO_2–EG nanofluid are given in Table 2. These properties are calculated using the following equations:

Effective thermal conductivity [32]:

$$k_{eff} = k_{static} + k_{Brownian} \quad (4)$$

$$k_{static} = k_f \left[\frac{(k_{np}+2k_f)-2\phi(k_f-k_{np})}{(k_{np}+2k_f)+\phi(k_f-k_{np})} \right] \quad (5)$$

Where k_{np} and k_f are the thermal conductivity of the solid particles and the base fluid respectively.

Thermal conductivity due to the Brownian motion presented by [33] as:

$$k_{Brownian} = 5\times10^4 \beta\phi p_f c_{pf} \sqrt{\frac{KT}{2R_{np}}} f(T,\phi) \quad (6)$$

$$f(T,\phi) = (0.028217\varnothing + 0.003917)\frac{T}{T_0} + (-0.030669\varnothing - 0.00391123)$$

Where K is the Boltzman constant, T is the fluid temperature; T_0 is the reference temperature, the β values for SiO_2 particle expressed in as follow [33]:

$$1.9526(100\phi) - 1.4594 \quad \text{for} \quad 1\% \le \varphi \le 10\% \quad \text{at} \quad 298K \le T \le 363K \quad (7)$$

The effective dynamic viscosity is given as [34]:

$$\frac{\mu_{eff}}{\mu_f} = \frac{1}{1-34.87(d_p/d_f)^{-0.3}\varnothing^{1.03}} \quad (8)$$

Where $$d_f = \left[\frac{6\times M}{N\times\pi\times\rho_{f0}} \right]^{1/3} \quad (9)$$

While μ_{eff} and μ_f are the viscosity of nanofluid and base fluid respectively, d_p is the nanoparticle diameter, d_f is the base fluid equivalent diameter and is the nanoparticle volume fraction. *M* is the molecular weight of the base fluid and *N* is the Avogadro number. ρ_{fo} is the mass density of the base fluid calculated at temperature T_0=293 K.

The effective density is given as [34]:

$$\rho_{eff} = (1-\varnothing)\rho_f + \varnothing\rho_s \quad (10)$$

Where ρ_{eff} and ρ_f are the nanofluid and base fluid densities respectively, and ρ_s is the density of nanoparticle.

The effective specific heat is given as [34]:

$$(Cp)_{eff} = \frac{(1-\varnothing)(\rho C_p)_f + \varnothing(\rho C_p)_s}{(1-\varnothing)\rho_f + \varnothing\rho_s} \quad (11)$$

Where Cp_s is the heat capacity of the solid particles and Cp_f is the heat capacity of the base fluid.

Table 2. Thermophysical properties of nanofluids.

	Base fluids	Nanoparticle
Properties	EG	SiO_2
ρ (kg/m^3)	1114.4	2200
μ (Nm/s)	0.0157	-
k (W/mK)	0.252	1.2
c_p (kJ/kgK)	2415	703

2.4 Numerical implementation

The Finite volume approach is used to solve the continuity, momentum and energy equations along with the corresponding boundary conditions. SIMPLE algorithm is used to solve the flow field inside the MT. The diffusion term in the momentum and energy equations is approximated by second-order central difference which gives a stable solution. The second-order upwind differencing scheme is considered for the convective terms. Five different sets of the grid sizes were imposed to the geometry and simulated by calculating the Nusselt number along the MT. The five grids sizes ($8\times6\times200$; $10\times8\times400$; $12\times10\times600$; $14\times12\times800$ and $16\times14\times1000$) show no much difference in the values of Nusselt number. The grid size of $14\times12\times800$ is selected in this study as it is found to provide a more stable solution. About the code validation part is documented in the Ref. [31].

3. RESULTS AND DISCUSSION

The simulations are performed for Reynolds number in the range of $10 \le Re \le 160$ and SiO_2 nanoparticle with pure EG as a base fluid. The nanoparticles volume fraction used was 0.04 with nanoparticles diameter 25nm. The MT used has a 100 mm length with different diameters ranged from 0.5 to 0.9 mm and different entrance sizes ranged from 0.371 to 2.5 mm. The heat flux that used to heat up the microtube was 50000 W/m^2. The inclination angles from the horizontal position were 0 °, ±45 °, ±90 °are used in this investigation.

Table 1. Summary of numerical and experimental studies for MT

Researchers	Diameter/ flow nature	Reynolds number	Fluid /gas	Findings
Zhou et al. [3]	50-1570 µm / laminar	20-2400	Deionized water	The Nusselt number along the axial direction did not accord with the conventional results.
Xiong and Chung [4]	50 µm/ laminar	40 - 2000	Water	The hydraulic diameter can result in increasing or decreasing the friction factor and Nu number.
Zhang et al. [5]	120-528 µm/ laminar	10-2280	Water	Heat transfer process is most sensitive to wall-to-fluid conductivity ration $k_{s/f}$.
Giulio and Paola [6]	50-150 µm/ laminar	100-1700	-	the influence of roughness on the heat transfer is smaller and more sensitive to the geometry of both duct and roughness obstruction and it is highly dependent on the tube shape.
Lelea et al. [7]	0.1-0.5 mm/ laminar	Up to 800	Distilled water	Results confirm that the conventional or classical theories are applicable for water flow through microchannel of above sizes.
Ding et al. [8]	6.35 mm/ laminar	700-1300	Distilled water / 0.5wt.% CNT	At Re=80 Reynolds number causes a significant increase 350% in the convective heat transfer coefficient
Yang and Lin [9]	123-962 µm/ laminar & turbulent	100-10000	Water	Heat loss of the total heat input depends on the inner diameter and the Reynolds number values
Kamali and Binesh [10]	1.55 mm/ laminar	600-1200	Water/ aqueous 1% CNT	Heat transfer coefficient was dominated by the wall region due to non-Newtonian behavior of CNT nanofluid.
Hong and Asako [11]	10-100 µm/ laminar	14-1829	Gas	A correlation for the prediction of the wall temperature of the gaseous flow in the MT was proposed.
Bianco et al. [12]	0.01m/ laminar	250-1050	Al_2O_3/water	Maximum difference detected was 11% for the average heat transfer coefficient especially for ∅= 4%.
Guo and Wu [13]	1-100 µm/ laminar and turbulent	100-1000	Gas	The local Nusselt number increased with increase the dimensionless length due to the compressibility effects.
Ghiaasiaan and Lak [14]	0.1 to 1 mm/ turbulent	5000-24000	-	Friction factors and heat transfer coefficients was higher than those predicted by macroscale models and correlations, while other indicated an opposite trends.
Celata et al [15]	70-326 µm/ laminar	Less than 300	Demineralised water	No effect of slip flow noted due to hydrophobic channel walls even at 70 µm inner diameter. For roughened glass channels, an increased in friction factor above 64/Re was observed only at the smallest diameter of 126 µm
Xiao et al. [16]	-	-	Gas	The maximum second-order changes of Nusselt number was on the order of 15%.
Peng et al. [17]	230 µm/ laminar & turbulent	1540-2960	Deionized water	The flow transition from laminar to turbulent occurs at Reynolds number 1700 to 1900
Celata et al. [18]	50-528 µm/ laminar and turbulent	50-3138	Demineralised water	The Nusselt number decreased with decreasing the diameter
Koo and Kleinstreuer [19]	50 µm/ laminar	20-2000	water, methanol and iso-propanol	Viscous dissipation effects could ultimately affect the friction factor measurements for flow in MT
Mala and Li [20]	50 to 254 µm/ turbulent	up to 2500	Water	The pressure gradient required to force the liquid through the MT was higher than that predicted by the conventional theory
Sara et al. [21]	0.20 mm/ laminar	40-1400	Distilled water	Friction factor was in a very good agreement with the Hagen-Poiseuille theory. The Sherwood number for MT was smaller than those obtained from the correlations developed for macrotubes.
Lelea and Cioabla [22]	0.1 mm/ laminar	7.2-1684	Water, HFE-7600 and FC-70	Friction factor and Poiseuille constant P_o affected on Nu at different values of Br
Satapathy [23]	-	-	gas	the dimensionless pressure drop increased with the increases of relative roughness, Reynolds number or wave number of wall function
Zhang and Fu [24]	0.531 and 1.042 mm	-	Nitrogen liquid	There was not yet a theoretical model which can predict the flow regime transition well for the two-phase flow
Wang and Wang [25]	-	1 to 500	-	The influence of wall roughness on the flow pattern was different from those on the pressure drop
Liu et al. [26]	242, 315 and 520 µm / laminar and turbulent	100-7000	Deionized water	Nusselt number is rough agreement with that of the laminar correlations
Celata et al. [27]	30-254 µm/ laminar	0.8-500	Helium	Friction factor has remarkably accurate prediction by Hagen-Poiseuille and effect of density-change-induced acceleration was extremely limited on the particle scale and that an incompressible characterization of flow
Aziz and Niedbalski [28]	-	-	Gas	As the viscous dissipation gathers strength, the Nusselt number reaches a minimum and then increases again as the effect of viscous dissipation continues to prevail over the cooling effect
Qi et al. [29]	0.531-1.931mm	-	Hitrogen liquid	Heat transfer coefficient increased with mass quality at low and medium heat fluxes
Wen and Ding [30]	4.5mm/laminar	500- 2100	Al_2O_3/water	Significant enhancement the convective heat transfer in the laminar flow regime and this enhancement increased with Reynolds number and the particle concentration.
Salman et al. [31], [37], [38]	50 µm / laminar	10-1500	Al_2O_3/EG CuO/EG SiO_2/EG ZnO/EG	SiO_2-EG nanofluid has the highest Nusselt number, followed by ZnO-EG, CuO-EG, Al_2O_3-EG, and lastly pure EG. The Nusselt number for all cases increases with the volume fraction but it decreases with the rise in the diameter of nanoparticles. In all configurations, the Nusselt number increases with Reynolds number.
Minea [36]	0.12 m/	500-2300	Al_2O_3/Water	The heat transfer coefficient of Al_2O_3/water nanofluids is increased by 3.4–27.8% under fixed Reynolds number compared with that of pure water.

3.1 Effect of tube diameter

The effect of tube geometry on, the axial and wall temperatures, axial velocity along the tube radius, Nusselt number and the pressure drop are presented in this section.

In Figure 1a and 1b temperature profile at z/L=1 along the tube radius and tube axis shows that the tube with 0.9 mm diameter has the highest temperature along the tube radius and tube wall followed by 0.7 mm, 0.5 mm respectively. This is because the velocity proportional inversely with the tube diameter. Smaller diameter increases the velocity which leads to decrease the temperature and vice versa.

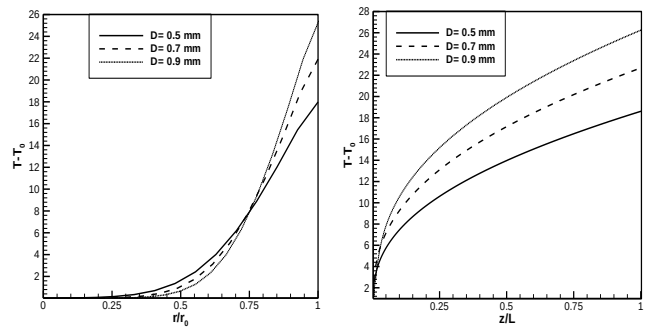

(a) (b)

Figure 1. Profiles of temperature at z/L=1for different tube diameters: (a) Temperature along the tube radius; (b) Temperature along tube axis

In Figure 2 the axial velocity along tube radius profile shows that the tube with 0.5 mm diameter has the highest

axial velocity along the tube radius at z/L=0.2 for Reynolds number Re=80 followed by 0.7 mm, then 0.9 mm. This is because the smaller tube diameter is proportional directly to the velocity.

Figure 3 shows the average Nusselt number for different Reynolds numbers. It can be obtained from this Figure that 0.9 mm has the highest Nusselt number comparing to other tubes. The larger tube diameter has highest Nusselt number. This is because for Nusselt number is proportional directly with the tube diameter; higher tube diameter leads to higher Nusselt number and vice versa. Figure 4 the pressure drop along the tube axis show that the tube with 0.5 mm diameter has the highest pressure drop followed by 0.7 mm and 0.9 mm. This is because the static pressure for the fluid is proportional directly with the velocity. Thus, 0.5 mm tube has the highest velocity which leads to increases the pressure drop.

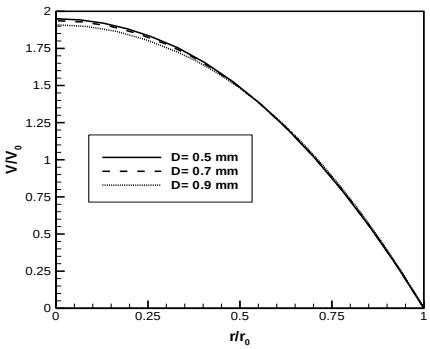

Figure 2. Profiles of axial velocity for different tube diameters at z =0.1 and Re= Re= 80

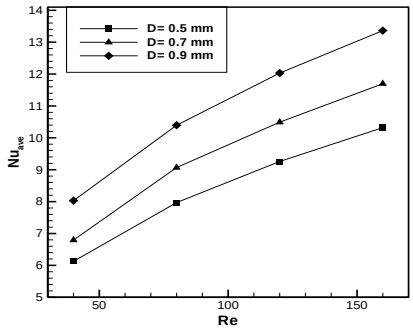

Figure 3. Average Nusselt number versus Reynolds number for different tube diameters

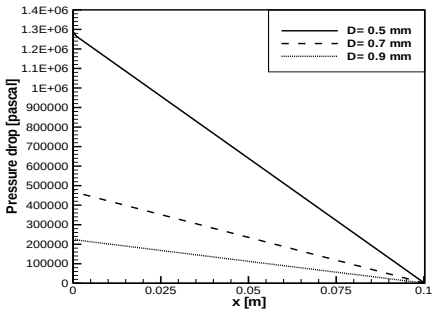

Figure 4. Pressure drop along the tube axis for different tube diameters at Re =80

3.2 Effect of entrance size

Three different entrance sizes were investigated in this section. The configuration for different entrance is illustrated in Figure 5. According to the entrance sizes three different diameters which is 0.371 mm, 0.9 mm and 2.5 mm were investigated. The results as shown in Figure 6 show that though the entrance region is just 40% from the tube length but it affects the heat transfer rate through the tube. It is evident that 2.5 mm entrance diameter has the highest Nusselt number followed by 0.9 mm, 0.371 mm respectively. This is because the Nusselt number is proportional directly with the entrance size.

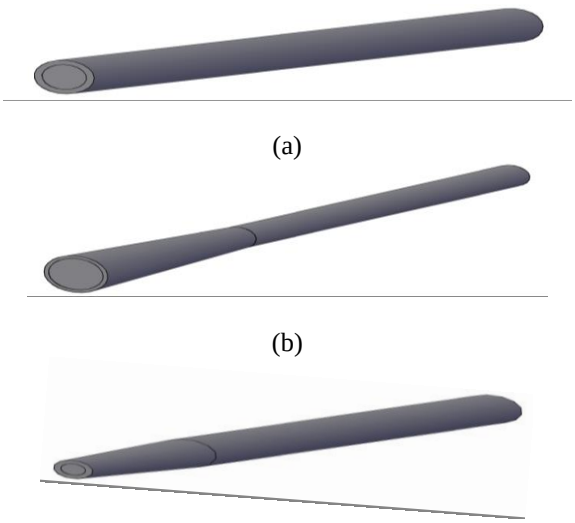

(a)

(b)

(c)

Figure 5. The configuration for different entrance sizes: (a) D= 0.9 mm; (b) D=2.5 mm; (c) D=0.371 mm

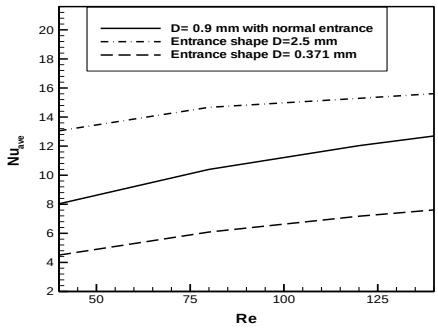

Figure 6. Average Nusselt number versus Reynolds number for different entrance sizes

3.3 Effect of inclination angles

Different inclination angles were investigated in this section. The configuration for different inclination angles is shown in Figure 7. The results for different inclination angles show no changes in the Nusselt number values and the pressure drop at different Reynolds numbers as shown in Table 3. This is because no effect of the gravity, the Richardson number which is a function of Grashof number divided on the Reynolds number is less than Ri < 0.1, so the natural convection is neglected and the forced convection is dominated.

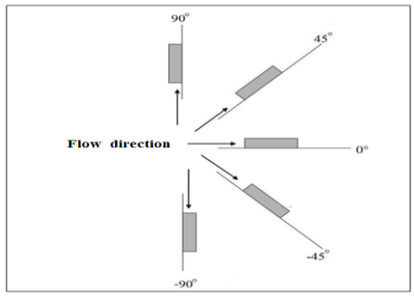

Figure 7. Configuration of microtube at different inclination angles

Table 3. The effects of inclination angle on Nusselt number average and pressure drop at different Reynolds number

(a) **At Reynolds number 10**

Angle	Nu_{ave}	Pressure
0 °	7.362852	79515.71
±45 °	7.362852	79515.71
±90 °	7.362852	79515.71

(b) **At Reynolds number 40**

Angle	Nu_{ave}	Pressure
0 °	10.11316	317295.8
±45 °	10.11316	317295.8
±90 °	10.11316	317295.8

(c) **At Reynolds number 80**

Angle	Nu_{ave}	Pressure
0 °	11.75585	638552.4
±45 °	11.75585	638552.4
±90 °	11.75585	638552.4

(d) **At Reynolds number 120**

Angle	Nu_{ave}	Pressure
0 °	12.86489	960093.9
± 45 °	12.86489	960093.9
± 90 °	12.86489	960093.9

4. CONCLUSIONS

The effect of geometrical parameters of microtube on the heat transfer enhancement was investigated numerically. It is concluded from the results that the heat transfer rate strongly depends on the geometry and the entrance size of the microtube. Higher tube diameter and entrance size have the highest Nusselt number and vice versa. No effects of inclination angle on heat transfer rate were found.

REFERENCES

1. S. Arcidiacono, N. R. Bieri, D. Poulikakos and C. P. Grigoropoulos, On the Coalescence of Gold Nanoparticles, *International Journal of Multiphase Flow*, vol. 30, pp. 979-994, 2004. DOI: 10.1016/j.ijmultiphaseflow.2004.03.006.
2. P. Buffat and J. P. Borel, Size Effect on Melting Temperature of Gold Particles, *Physical Review A*, vol. 13(6), pp. 2287-2298, 1976. DOI: 10.1103/PhysRevA.13.2287.
3. Zhuo Li, Ya-Ling He, Gui-Hua Tang, Wen-Quan Tao, Experimental and Numerical Studies of Liquid Flow and Heat Transfer in Microtubes, *Int. J. Heat and Mass Transfer*, vol. 50, pp. 3447–3460, 2007. DOI: 10.1016/j.ijheatmasstransfer.2007.01.016.
4. Renqiang Xiong, J. N. Chung, A New Model for Three-Dimensional Random Roughness Effect on Friction Factor and Heat Transfer in Microtubes, *Int. J. Heat and Mass Transfer*, vol. 53, pp. 3284–3291, 2010. DOI: 10.1016/j.ijheatmasstransfer.2010.02.050.
5. Sun-Xiao Zhang, Ya-Ling He, Guy Lauriat and Wen-Quan Tao, Numerical Studies of Simultaneously Developing Laminar Flow and Heat Transfer in Microtubes with Thick Wall and Constant Outside Wall Temperature, *Int. J. Heat and Mass Transfer*, vol. 53, pp. 3977–3989, 2010. DOI: 10.1016/j.ijheatmasstransfer.2010.05.017.
6. Giulio and Paola, Numerical Analysis of Roughness Effect on Microtube Heat Transfer, *J. Superlattices and Microstructures*, vol. 35, pp. 601–616, 2004. DOI: 10.1016/j.spmi.2003.09.014.
7. Dorin Lelea, Shigefumi Nishio and Kiyoshi Takano, The Experimental Research on Microtube Heat Transfer and Fluid Flow Of Distilled Water, *Int. J. Heat and Mass Transfer*, vol. 47, pp. 2817–2830, 2004. DOI: 10.1016/j.ijheatmasstransfer.2003.11.034.
8. Yulong Ding, Hajar Alias, Dongsheng Wen and Richard A. Williams, Heat transfer of aqueous suspensions of carbon nanotubes (CNT nanofluids), *Int. J. Heat and Mass Transfer*, vol. 49, pp. 240–250, 2006. DOI: 10.1016/j.ijheatmasstransfer.2005.07.009.
9. C. Y. Yang, T. Y. Lin, Heat Transfer Characteristics of Water Flow in Microtubes, *Experimental Thermal and Fluid Science*, vol. 32, pp. 432–439, 2007. DOI: 10.1016/j.expthermflusci.2007.05.006.
10. R. Kamali, A. R. Binesh, Numerical Investigation of Heat Transfer Enhancement Using Carbon Nanotube-Based Non-Newtonian Nanofluids, *Int. Comm. Heat and Mass Transfer*, vol. 37, pp. 1153–1157, 2010. DOI: 10.1016/j.icheatmasstransfer.2010.06.001.
11. Chungpyo Hong, Yutaka Asako, Heat Transfer Characteristics of Gaseous Flows in Microtube with Constant Heat Flux, *Applied Thermal Engineering*, vol. 28, pp. 1375–1385, 2008. DOI: 10.1016/j.applthermaleng.2007.10.006.
12. V. Bianco, F. Chiacchio, O. Manca, S. Nardini, Numerical Investigation of Nanofluids Forced Convection in Circular Tubes, *Applied Thermal Engineering*, vol. 29, pp. 3632–3642, 2009. DOI: 10.1016/j.applthermaleng.2009.06.019.
13. Z. Y. GUO and X. B, WU. Compressibility effect on the gas flow and heat transfer in a microtube. *Int. J. Heat and Mass Transfer*, vol. 40, pp. 3251-3254, 1996. DOI: 10.1016/S0017-9310(96)00323-7.
14. S. M. Ghiaasiaan, T. S. Laker, Turbulent Forced Convection in Microtubes, *Int. J. Heat and Mass Transfer*, vol. 44, pp. 2777-2782, 2001. DOI: 10.1016/S0017-9310(00)00320-3.
15. G. P. Celata, M. Cumo, S. McPhail, G. Zummo, Characterization of Fluid Dynamic Behavior and Channel Wall Effects in Microtube, *Int. J. Heat and Mass Transfer*, vol. 27, pp. 135–143, 2006. DOI: 10.1016/j.ijheatfluidflow.2005.03.012.
16. Nian Xiao, John Elsnab, Tim Ameel, Microtube Gas Flows with Second-Order Slip Flow and Temperature Jump Boundary Conditions, *Int. J. Thermal Sciences*, vol. 48, pp. 243–251, 2009. DOI: 10.1016/j.ijthermalsci.2008.08.007.
17. Peng-Fei Hao, Xi-Wen Zhang, Zhao-Hui Yao, Feng He. Transitional and Turbulent Flow in a Circular Microtube, *Experimental Thermal and Fluid Science*, vol. 32, pp. 423–431, 2007. DOI: 10.1016/j.expthermflusci.2007.05.004.
18. G. P. Celata, M. Cumo, V. Marconi, S. J. McPhail, G. Zummo, Microtube Liquid Single-Phase Heat Transfer in Laminar Flow, *Int. J. Heat and Mass Transfer*, vol. 49, pp. 3538–3546, 2006. DOI: 10.1016/j.ijheatmasstransfer.2006.03.004.
19. J. Koo, C. Kleinstreuer, Viscous Dissipation Effects in Microtubes and Microchannels, *Int. J. Heat and Mass Transfer*, 47:3159–3169, 2004. DOI: 10.1016/j.ijheatmasstransfer.2004.02.017.
20. Gh. Mohiuddin Mala, Dongqing Li, Flow Characteristics of Water in Microtubes, *Int. J. Heat and Fluid Flow*, vol. 20, pp.142-148, 1999. DOI: 10.1016/S0142-727X(98)10043-7.
21. O. N. Sara, O. Barlay Ergu, M. E. Arzutug, S. Yapici, Experimental Study of Laminar Forced Convective Mass Transfer and Pressure Drop in Microtubes, *Int. J. Thermal Sciences*, vol. 48, pp. 1894–1900, 2009. DOI: 10.1016/j.ijthermalsci.2009.01.021.
22. Dorin Lelea, Adrian Eugen Cioabla, The Viscous Dissipation Effect on Heat Transfer and Fluid Flow in Micro-Tubes, Int. Comm. *Heat and Mass Transfer*, vol. 37, pp. 1208–1214, 2010. DOI: 10.1016/j.icheatmasstransfer.2010.06.030.
23. Ashok K. Satapathy, Slip Flow Heat Transfer in an Infinite Microtube with Axial Conduction, *Int. J. Thermal Sciences*, vol. 49, pp. 153–160, 2010. DOI: 10.1016/j.ijthermalsci.2009.06.012.

24. P. Zhang, X. Fu, Two-Phase Flow Characteristics of Liquid Nitrogen in Vertically Upward 0.5 And1.0 Mm Micro-Tubes: *Visualization Studies, Cryogenics*, vol. 49, pp. 565–575, 2009. DOI: 10.1016/j.cryogenics.2008.10.017.
25. Haoli Wang, Yuan Wang, Influence of Three-Dimensional Wall Roughness on the Laminar Flow in Microtube, *Int. J. Heat and Fluid Flow*, vol. 28, pp. 220–228, 2007. DOI: 10.1016/j.ijheatfluidflow.2006.08.005.
26. Zhi-Gang Liu, Shi-Qiang Liang, Masahiro Takei, Experimental Study on Forced Convective Heat Transfer Characteristics in Quartz Microtube, *Int. J. Thermal Sciences*, vol. 46, pp.139–148, 2007. DOI: 10.1016/j.ijthermalsci.2006.03.008.
27. G. P. Celata, M. Cumo, S. J. McPhail, L. Tesfagabir, G. Zummo, Experimental Study on Compressible Flow in Microtubes. *Int. J. Heat and Fluid Flow*, vol. 28, pp. 28–36, 2007. DOI: 10.1016/j.ijheatfluidflow.2006.04.009.
28. A. Aziz, Nick Niedbalski, Thermally Developing Microtube Gas Flow with Axial Conduction and Viscous Dissipation, *Int. J. Thermal Sciences*, vol. 50, pp. 332–340, 2011. DOI: 10.1016/j.ijthermalsci.2010.08.003.
29. S. L. Qi, P. Zhang, R. Z. Wang, L. X. Xu, Flow Boiling of Liquid Nitrogen in Micro-Tubes: Part II–Heat Transfer Characteristics and Critical Heat Flux, *Int. J. Heat and Mass Transfer*, vol. 50, pp. 5017–5030, 2007. DOI: 10.1016/j.ijheatmasstransfer.2007.08.017.
30. Dongsheng Wen, Yulong Ding, Experimental Investigation into Convective Heat Transfer of Nanofluids at the Entrance Region under Laminar Flow Conditions, *Int. J. Heat and Mass Transfer*, vol. 47, pp. 5181–5188, 2004. DOI: 10.1016/j.ijheatmasstransfer.2004.07.012.
31. B. H. Salman, H. A. Mohammed, A. SH. Kherbeet, Heat Transfer Enhancement of Nanofluids Flow in Microtube With Constant Heat Flux, J. *Int. Comm. Heat and Mass Transfer*, vol. 39, pp. 1195-1204, 2012. DOI: 10.1016/j.icheatmasstransfer.2012.07.005.
32. B. Ghasemi, S. Aminossadati, Brownian Motion of Nanoparticles in a Triangular Enclosure with Natural Convection, *J. Thermal Sciences*, vol. 49,pp. 931–940, 2010. DOI: 10.1016/j.ijthermalsci.2009.12.017.
33. R. S. Vajjha, D. K. Das, Experimental Determination of Thermal Conductivity of Three Nanofluids and Development of New Correlations, *J. Heat and Mass Transfer*, vol. 52, pp. 4675–4682, 2009. DOI: 10.1016/j.ijheatmasstransfer.2009.06.027.
34. M. Corcione, Heat Transfer Features of Buoyancy-Driven Nanofluids inside Rectangular Enclosures Differentially Heated at the Sidewalls, *J. Thermal Sciences*, vol. 49, pp. 1536–1546, 2010. DOI: 10.1016/j.ijthermalsci.2010.05.005.
35. S.V. Patankar, Numerical Heat Transfer and Fluid Flow, Hemisphere, New York, 1980
36. A. A. Minea, Effect of Microtube Length on Heat Transfer Enhancement of a Water/Al_2O_3 Nanofluid at High Reynolds Numbers, *Int. J. Heat and Mass Transfer*, vol. 62, pp. 22-30, 2013. DOI: 10.1016/j.ijheatmasstransfer.2013.02.057.
37. B. H. Salman, H. A. Mohammed, K. M. Munisamy, A. Sh. Kherbeet, Characteristics of Heat Transfer and Fluid Flow in Microtube and Microchannel Using Conventional Fluids and Nanofluids: *A Review: Renewable and Sustainable Energy Reviews*, vol. 28, pp. 848-880, 2013. DOI: 10.1016/j.rser.2013.08.012.
38. B. H. Salman, H. A. Mohammed, K. M. Munisamy, A. Sh. Kherbeet, Three-Dimensional Numerical Investigation of Nanofluids Flow in Microtube with Different Values of Heat Flux, *Heat Transfer—Asian Research*, 2014. DOI: 10.1002/htj.21139.

NOMENCLATURE

Al_2O_3	Aluminum oxide
C_p	Specific heat of the fluid, J/kgK
CuO	Copper oxide
d_f	Diameter of base fluid molecule
d_p	Nanoparticle diameter, m
g	Gravitational acceleration, m/s^2
k	Thermal conductivity, W/mK
k_{eff}	Effective thermal conductivity
L	Length of the tube, m
M	Molecular weight of base fluid
Avogadro No,	$N = 6.022x10^{23} mol^{-1}$
Nu	Nusselt number,
P	Pressure of fluid, Pa
Pr	Prandtl number, $Pr = Cp\ \mu_0/k$
q_x	Heat flux, W/m^2
Re	Reynolds number, $Re = \rho_0 V_0 D/\mu_0$
R_{np}	Nanoparticle radius, m
Ri	Richardson number, $Ri = Gr/Re$
SiO_2	Silicon oxide
T	Temperature of fluid, K
T	Bulk temperature, K
T_0	Reference temperature
Velocities in x ´, y ´and z ´directions, m/s	
Dimensionless velocities in x, y and z directions	
Average jet velocity at the entrance, m/s	
V	Axial velocity, m/s
Zinc oxide	

Greek symbols

μ_{eff}	Effective viscosity
α	Thermal diffusivity, m^2/s
μ	Dynamic viscosity of fluid, $kg/m\ s$
υ	Kinematic viscosity of fluid, $m^2\ s$
θ	Inclination of tilted wall
ρ	Fluid density, kg/m^3
ρ_1	Nanofluid density kg/m^3
φ	Volume fraction of nanoparticles

Subscript

b_f	base-fluid
n_f	nanofluids
n_p	nanoparticle
eff	effective